Octahedral Iridium Clusters: Synthesis, Electrochemical Mechanisms of Formation, and Solid-State Structures of $[Ir_6(CO)_{14}(\mu\text{-TePh})]^-$ and $[Ir_6(CO)_{13}(\mu\text{-TePh})_2]$

Roberto Della Pergola,*,† Alessandro Ceriotti,† Arnaldo Cinquantini,‡ Fabrizia Fabrizi de Biani,‡ Luigi Garlaschelli,† Mario Manassero,*,§ Rossana Piacentini,† Mirella Sansoni,§ and Piero Zanello*,‡,||

Dipartimento di Chimica Inorganica, Metallorganica ed Analitica and Centro del CNR and Dipartimento di Chimica Strutturale e Stereochimica Inorganica, via G. Venezian 21, 20133 Milano, Italy, and Dipartimento di Chimica dell'Università di Siena, Pian dei Mantellini 44, 53100 Siena, Italy

Received July 21, 1997

The diphenyl ditelluride PhTeTePh reacts with $[Ir_6(CO)_{15}]^{2-}$ (in refluxing tetrahydrofuran) or $Ir_6(CO)_{16}$ (in toluene) yielding $[Ir_6(CO)_{14}(\mu\text{-TePh})]^-$ or $[Ir_6(CO)_{13}(\mu\text{-TePh})_2]$, respectively. Analogous mono- and disubstituted iridium compounds were prepared with other diaryl disulfides or diselenides. Electrochemical experiments confirm the different reactivity of PhTeTePh and PhSSPh showing that the ditelluride adds to the electrogenerated transient radical $[Ir_6(CO)_{15}]^{-\bullet}$ and the disulfide to $[Ir_6(CO)_{15}]^0$. The two clusters consists of octahedra of iridium atoms with one or two edges bridged by phenyltellurolate ligands. The Ir−Ir bonds trans to the TePh unit are remarkably short.

The chemistry of transition metal complexes with main-group elements is rapidly expanding.[1] Metal clusters and chalcogenide ligands are nowadays frequently combined,[2] and many different applications are documented: several representative examples can be found in the literature such as (i) the use of the cluster $[Rh_{10}Se(CO)_{22}]^{2-}$, supported on TiO_2, for the selective hydrogenation of CO_2 to ethanol,[3] (ii) the synthesis of Pt/Re/S clusters, used as model compounds for the understanding of the role of the three elements in petroleum reforming;[4] (iii) the assembly of two-dimensional ordered arrays of gold particles with dithiolate ligands,[5] and (iv) the formation of extended materials by decomposition of the molecular precursor, to be used in microelectronics.[2,6]

The coordination of SePh units on carbonyl clusters was previously documented by the characterization of $Ru_6C(CO)_{14}(\mu\text{-SePh})_2$ and other related derivatives.[7] Very little is known about iridium clusters containing group 16 ligands,[8] with the exception of Ir−S and Ir−Se complexes;[9] therefore, we investigated the synthesis of Ir−Te compounds, focusing on the reactivity of diphenylditelluride PhTeTePh[10] (**1**) with tetra- and hexanuclear clusters.

The anionic cluster $[Ir_6(CO)_{14}(\mu\text{-TePh})]^-$ (**2**) can be obtained by refluxing PhTeTePh and $[Ir_6(CO)_{15}]^{2-}$ (molar ratio > 3) in tetrahydrofuran (THF), eq 1. The

$$[Ir_6(CO)_{15}]^{2-} + PhTeTePh \rightarrow [Ir_6(CO)_{14}(\mu\text{-TePh})]^- + PhTe^- + CO \quad (1)$$

reaction is very selective but slow, requiring more than 20 h to be completed. The infrared spectra of **2** in the carbonyl region is strongly reminiscent of that of halogen-substituted hexanuclear iridium clusters[11,12] and was used to infer the correct formula of the reaction product and the stoichiometry of the whole process, which involves formal oxidation of the cluster. This reaction strictly recalls the formation of $[Ir_6(CO)_{14}(\mu\text{-I})]^-$, which occurs rapidly at room temperature owing to the high oxidizing power of iodine, eq 2.[11] The

$$[Ir_6(CO)_{15}]^{2-} + I_2 \rightarrow [Ir_6(CO)_{14}(\mu\text{-I})]^- + I^- + CO \quad (2)$$

addition of oxidizing agents, such as ferrocenium or tropylium cations, was indeed necessary in order to obtain analogous clusters substituted by phenylthiolate or -selenolate.

Thus, when treating $[Ir_6(CO)_{15}]^{2-}$ with large excesses of $[Fe(C_5H_5)_2]PF_6$ and diphenyldisulfide (molar ratio 1:5:2), the main product is the monoanion $[Ir_6(CO)_{14}(\mu$-

† Dipartimento di Chimica Inorganica, Metallorganica ed Analitica.
‡ Dipartimento di Chimica dell'Università di Siena.
§ Dipartimento di Chimica Strutturale e Stereochimica Inorganica.
|| E-mail: zanello@unisi.it.

(1) Whitmire, K. H. *J. Coord. Chem.* **1988**, *17*, 95.
(2) Dance, I.; Fisher, K. *Prog. Inorg. Chem.* **1994**, *41*, 637.
(3) Kurakata, H.; Izumi, Y.; Aika, K. *J. Chem. Soc., Chem. Commun.* **1996**, 389.
(4) Hao, L.; Xiao, J.; Vittal, J. J.; Puddephatt, R. J. *Organometallics* **1997**, *16*, 2165.
(5) Andres, R. P.; Bielefeld, J. D.; Henderson, J. I.; Janes, D. B.; Kolagunta, V. R.; Kubiak, C. P.; Mahoney, W. J.; Osifchin; R. G. *Science* **1996**, *273*, 1690.
(6) Steigerwald, M. L.; Stuczysnki, S. M.; Kwon, Y.-U.; Vennos, D. A.; Brennan, J. G. *Inorg. Chim. Acta* **1993**, *212*, 219.
(7) Chihara, T.; Yamazaki, H. *J. Organomet. Chem.* **1992**, *428*, 169.
(8) Arnold, J. *Prog. Inorg. Chem.* **1995**, *43*, 353.
(9) Della Pergola, R.; Garlaschelli, L.; Martinengo, S.; Demartin, F.; Manassero, M.; Sansoni, M. *J. Chem. Soc., Dalton Trans.* **1986**, 2463.
(10) Petragnani, N. In *Comprehensive Organometallic Chemistry II*; Abel, E. W., Stone, F. G. A., Wilkinson, G., Eds.; Pergamon Press: Oxford, 1995; Vol. 11, p 603.
(11) Della Pergola, R.; Garlaschelli, L.; Martinengo, S.; Demartin, F.; Manassero, M.; Masciocchi, N. *J. Chem. Soc., Dalton Trans.* **1988**, 2307.
(12) Della Pergola, R.; Garlaschelli, L.; Martinengo, S.; Demartin, F.; Manassero, M.; Masciocchi, N.; Bau, R.; Zhao, D. *J. Organomet. Chem.* **1990**, *396*, 385.

S0276-7333(97)00621-3 CCC: $15.00
Publication on Web 01/31/1998

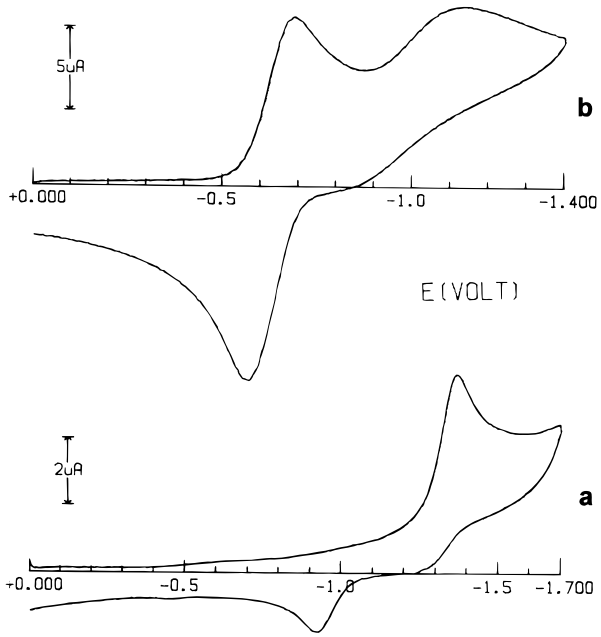

Figure 1. Cyclic voltammetric responses recorded at a platinum electrode on CH_2Cl_2 solutions containing $[NBu_4][PF_6]$ (0.2 mol dm^{-3}) and (a) **2** (5×10^{-4} mol dm^{-3}) or (b) **3** (8×10^{-4} mol dm^{-3}). Scan rate = 0.2 Vs^{-1}.

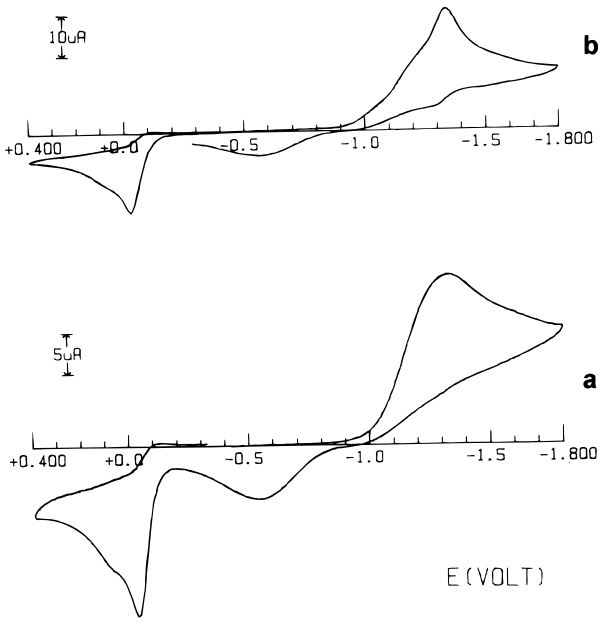

Figure 2. Cyclic voltammetric responses recorded at a platinum electrode on CH_2Cl_2 solutions containing $[NBu_4][PF_6]$ (0.2 mol dm^{-3}) and a 1:1 mixture of $[Ir_6(CO)_{15}]^{2-}$ and PhTeTePh (1.0×10^{-3} mol dm^{-3}): (a) cathodic scan; (b) anodic scan. Scan rate = 0.2 Vs^{-1}.

SPh)]$^-$. With such a large amount of the oxidant, only low yields of neutral $[Ir_6(CO)_{13}(SPh)_2]$ are achieved. The two clusters could be easily separated by solvent extraction and could be identified by their elemental analysis and spectroscopic properties. Using the same experimental conditions, with the same ratios, **1** and $[Ir_6(CO)_{15}]^{2-}$ yield mainly $[Ir_6(CO)_{13}(\mu\text{-TePh})_2]$ (**3**), emphasizing the different behavior of the two dichalcogenides. However, we found that the best way to prepare the neutral cluster **3** is the reaction of diphenyl ditelluride and $Ir_6(CO)_{16}$ in refluxing toluene. The process can be represented by eq 3. The same reaction of $[Ir_6(CO)_{16}]$

$$[Ir_6(CO)_{16}] + \text{PhTeTePh} \rightarrow [Ir_6(CO)_{13}(\mu\text{-TePh})_2] + 3CO \quad (3)$$

and disulfides or diselenides is much less selective, producing mixtures of mono- and disubstituted (yields 30%) clusters, such as $[Ir_6(CO)_{13}(SeCH_2Ph)_2]$.

Electrochemistry. We have performed an electrochemical investigation on either **2**, **3**, or mixtures of $[Ir_6(CO)_{15}]^{2-}$ and diphenyl ditelluride, shedding light on the redox pathways leading to complexes **2** and **3**. Figure 1a and b shows the redox fingerprint of clusters **2** and **3**, respectively.

Controlled-potential coulometric tests show that anion **2** undergoes an irreversible two-electron reduction (E_p = −1.37 V), whereas complex **3** first undergoes a chemically reversible, one-electron reduction ($E^{\circ\prime}$ = −0.62 V) followed by a second, irreversible, one-electron reduction (E_p = −1.13 V).

In order to understand how **2** and **3** may arise from reaction of $[Ir_6(CO)_{15}]^{2-}$ and PhTeTePh, it is useful to keep in mind the redox profiles of such reagents. The dianion $[Ir_6(CO)_{15}]^{2-}$ undergoes two subsequent one-electron oxidations ($E^{\circ\prime}_{2-/-}$ = −0.05 V; $E^{\circ\prime}_{-/0}$ = +0.14 V), the first of which is chemically reversible whereas the second one is followed by chemical complications.[13] PhTeTePh undergoes an irreversible two-electron reduction (E_p = −1.26 V) as well as a one-electron oxidation coupled to chemical complications ($E^{\circ\prime}_{0/+}$ = +0.75 V).

Let us now discuss the voltammetric diagrams illustrated in Figure 2, which refer to a 1:1 mixture of $[Ir_6(CO)_{15}]^{2-}$ and PhTeTePh. Starting from the resting potential (0.5 V) and scanning toward negative potential values (Figure 2a), the unaltered response of PhTeTePh appears, but the reverse scan points out that the oxidation path of $[Ir_6(CO)_{15}]^{2-}$ is strongly altered, *i.e.*, the first oxidation becomes irreversible (complicated by fast chemical reactions) and the second oxidation disappears. This is confirmed by the scanning toward positive values directly, Figure 2b. In addition, as a consequence of the chemical complications following the $[Ir_6(CO)_{15}]^{2-/-}$ step, the irreversible reduction of **2** becomes rather well detectable in the reverse scan (E_p = −1.37 V), notwithstanding the overlapping presence of the PhTeTePh reduction. As a matter of fact, exhaustive one-electron oxidation at +0.3 V affords **2**. These data suggest the occurrence of the following overall mechanism.

$$[Ir_6(CO)_{15}]^{2-} \rightleftarrows [Ir_6(CO)_{15}]^- + e^-$$

$$2[Ir_6(CO)_{15}]^- + \text{PhTeTePh} \rightarrow \{\text{unidentified products}\} \rightarrow 2[Ir_6(CO)_{14}(\text{TePh})]^- + 2CO$$

Even more explicative are the redox paths illustrated in Figure 3. As shown, upon reversing the potential scan after traversing the most anodic peaks due to successive oxidation processes of the (unidentified)

(13) Cinquantini, A.; Zanello, P.; Della Pergola, R.; Garlaschelli, L.; Martinengo, S. *J. Organomet. Chem.* **1991**, *412*, 215.

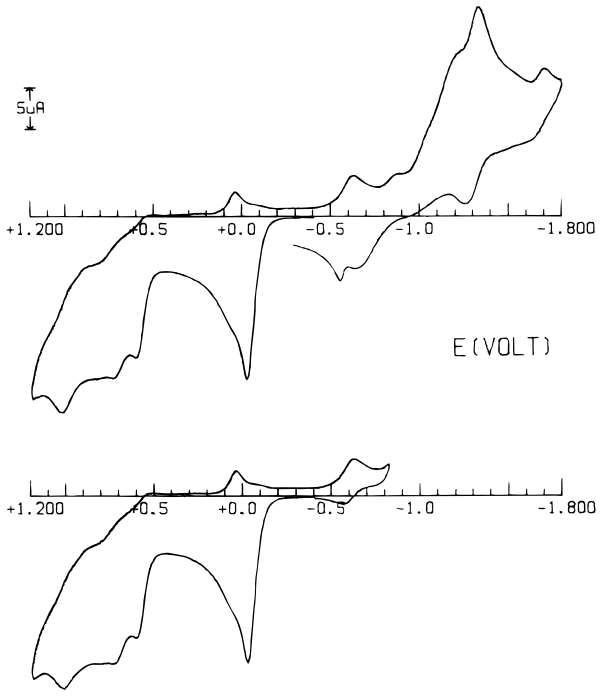

Figure 3. Cyclic voltammograms recorded under the same experimental conditions as Figure 2, extending the anodic scan up to the highest detected oxidation processes.

primary product arising from reaction between $[Ir_6(CO)_{15}]^-$ and PhTeTePh ($E_p \approx 1$ V), not only the reduction step of **2** becomes well evident ($E_p = -1.37$ V) but also the peak system of the reversible reduction of **3** appears ($E^{o\prime} = -0.62$ V). As proof of the complexity of the reaction pattern governing the formation of **3**, which does not allow us to propose the underlying electrode mechanism, it must be noted that reversing the potential scan after traversing the less anodic peaks at +0.6 and +0.7 V, respectively, the reduction process of **3** does not appear.

Finally, we wish to briefly account for the different, low reactivity of $[Ir_6(CO)_{15}]^{2-}$ toward PhSSPh. Granted that PhSSPh does not exhibit redox processes in the region from +1.2 to −1.9 V, mixtures of $[Ir_6(CO)_{15}]^{2-}$ and PhSSPh give rise to voltammetric profiles[14] which show that the instantaneously electrogenerated monoanion $[Ir_6(CO)_{15}]^-$ is not involved in reactions with PhSSPh. From a comparison with the response of pure $[Ir_6(CO)_{15}]^{2-}$, a minor involvement of $[Ir_6(CO)_{15}]^0$ can be proposed, in that the directly associated re-reduction almost disappears, giving rise to an irreversible reduction at $E_p = -1.32$ V, which we assign as the reduction of $[Ir_6(CO)_{14}(SPh)]^-$.

In summary, electrochemical observations and chemical evidences are in total agreement, showing that (i) addition of the phenylchalcogenolate occurs upon oxidation of the $[Ir_6(CO)_{15}]^{2-}$ cluster, (ii) ditelluride and disulfide react by different paths (PhTeTePh reacts fastly with the monoanion $[Ir_6(CO)_{15}]^-$, PhSSPh slowly reacts with the neutral species $[Ir_6(CO)_{15}]^0$) and different selectivity, and (iii) after two-electron oxidations, either $[Ir_6(CO)_{13}(TePh)_2]$ or $[Ir_6(CO)_{14}(SPh)]^-$ is formed preferentially.

(14) Figure 1s in the Supporting Information.

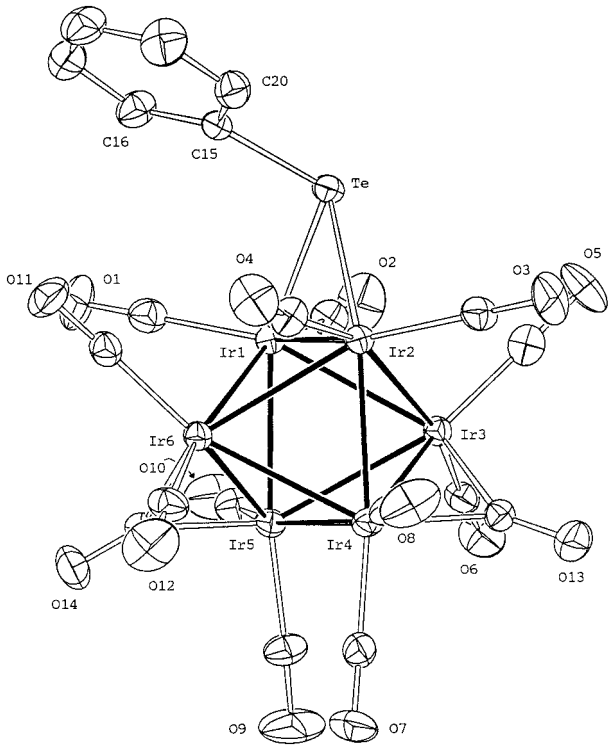

Figure 4. Solid-state structure of $[Ir_6(CO)_{14}(\mu\text{-TePh})]^-$ (**2**). Ellipsoids are drawn at the 30% probability level. The carbon atoms are labeled as the oxygen to which they are attached.

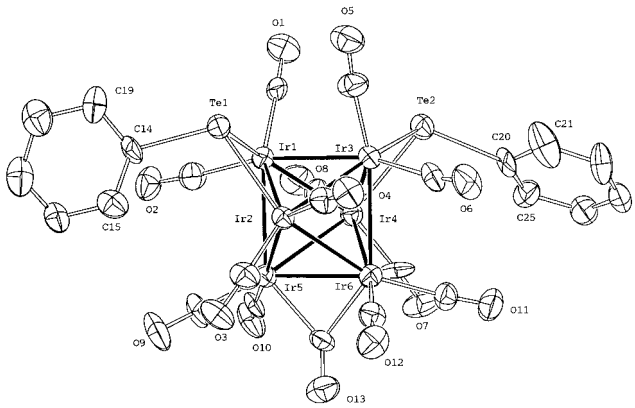

Figure 5. Solid-state structure of $[Ir_6(CO)_{13}(\mu\text{-TePh})_2]$ (**3**). Ellipsoids are drawn at the 30% probability level. The carbon atoms are labeled as the oxygen to which they are attached.

Crystal Structures of $[PPh_4][Ir_6(CO)_{12}(\mu\text{-CO})_2(\mu\text{-TePh})]$ (2a) and $[Ir_6(CO)_{12}(\mu\text{-CO})(\mu\text{-TePh})_2]$ (3). The solid-state structures of clusters **2** and **3** are shown in Figures 4 and 5, and selected bond distances and angles are listed in Tables 1 and 2. In both clusters, the six iridium atoms define an octahedron, having one (in **2**) or two (in **3**) edges bridged by the tellurium atoms. All iridium vertices are bound to two terminal carbonyl ligands; two or one bridging carbonyls, respectively, connect the metal atoms that are not bound to the phenyltellurolate fragments.

The coordination around the tellurium atoms is always pyramidal, with Ir−Te−C angles of 105−110°, owing to the presence of a lone pair on each group 16 atom. Cluster **3** possesses an idealized C_2 symmetry, with the axis defined by C(13) and the midpoint of the

Table 1. Selected Distances (Å) and Angles (deg) in $[Ir_6(CO)_{14}(\mu\text{-TePh})]^-$[a]

Metal−Metal Distances			
Ir(1)−Ir(2)	2.738(1)	Ir(2)−Ir(6)	2.768(1)
Ir(1)−Ir(3)	2.771(1)	Ir(3)−Ir(4)	2.738(1)
Ir(1)−Ir(5)	2.707(1)	Ir(3)−Ir(5)	2.796(1)
Ir(1)−Ir(6)	2.786(1)	Ir(4)−Ir(5)	2.840(1)
Ir(2)−Ir(3)	2.775(1)	Ir(4)−Ir(6)	2.793(1)
Ir(2)−Ir(4)	2.708(1)	Ir(5)−Ir(6)	2.746(1)
Ir−C_{term} Distances			
Ir(1)−C(1)	1.89(1)	Ir(4)−C(7)	1.88(1)
Ir(1)−C(2)	1.88(1)	Ir(4)−C(8)	1.83(1)
Ir(2)−C(3)	1.88(1)	Ir(5)−C(9)	1.87(1)
Ir(2)−C(4)	1.89(1)	Ir(5)−C(10)	1.86(1)
Ir(3)−C(5)	1.83(1)	Ir(6)−C(11)	1.87(1)
Ir(3)−C(6)	1.87(1)	Ir(6)−C(12)	1.88(1)
Ir−C_{br} Distances			
Ir(3)−C(13)	2.06(1)	Ir(5)−C(14)	2.08(1)
Ir(4)−C(13)	2.06(1)	Ir(6)−C(14)	2.05(1)
Other Distances			
Ir(1)−Te	2.620(1)	C_{term}−O_{term} (average)	1.14
Ir(2)−Te	2.612(1)	C_{br}−O_{br} (average)	1.16
Te−C(15)	2.12(1)		
Angles			
Ir(1)−Te−Ir(2)	63.12(2)	Ir(2)−Te−C(15)	105.1(3)
Ir(5)−Ir(1)−Te	148.81(2)	Ir−C_{term}−O_{term} (average)	177
Ir(4)−Ir(2)−Te	148.75(2)	Ir−C_{br}−O_{br} (average)	138
Ir(1)−Te−C(15)	108.8(3)		

[a] Estimated standard deviations are given in parentheses. Abbreviations: term = terminal; br = edge bridging.

Table 2. Selected Distances (Å) and Angles (deg) in $[Ir_6(CO)_{13}(\mu\text{-TePh})_2]$[a]

Metal−Metal Distances			
Ir(1)−Ir(2)	2.744(2)	Ir(2)−Ir(6)	2.721(2)
Ir(1)−Ir(3)	2.759(2)	Ir(3)−Ir(4)	2.751(2)
Ir(1)−Ir(4)	2.749(2)	Ir(3)−Ir(6)	2.784(2)
Ir(1)−Ir(5)	2.766(2)	Ir(4)−Ir(5)	2.703(2)
Ir(2)−Ir(3)	2.729(2)	Ir(4)−Ir(6)	2.811(2)
Ir(2)−Ir(5)	2.833(2)	Ir(5)−Ir(6)	2.782(2)
Ir−C_{term} Distances			
Ir(1)−C(1)	1.88(2)	Ir(4)−C(7)	1.89(3)
Ir(1)−C(2)	1.91(3)	Ir(4)−C(8)	1.86(3)
Ir(2)−C(3)	1.78(3)	Ir(5)−C(9)	1.92(2)
Ir(2)−C(4)	1.92(3)	Ir(5)−C(10)	1.87(2)
Ir(3)−C(5)	1.81(3)	Ir(6)−C(11)	1.91(3)
Ir(3)−C(6)	1.91(3)	Ir(6)−C(12)	1.79(3)
Ir−C_{br} Distances			
Ir(5)−C(13)	2.08(3)	Ir(6)−C(13)	2.04(3)
Other Distances			
Ir(1)−Te(1)	2.600(2)	Te(1)−C(14)	2.11(2)
Ir(2)−Te(1)	2.621(2)	Te(2)−C(20)	2.13(3)
Ir(3)−Te(2)	2.601(2)	C_{term}−O_{term} (average)	1.13
It(4)−Te(2)	2.631(2)	C(13)−O(13)	1.15(4)
Angles			
Ir(1)−Te(1)−Ir(2)	63.44(5)	Ir(5)−Ir(4)−Te(2)	148.58(6)
Ir(3)−Te(2)−Ir(4)	63.45(5)	Ir−Te−C (average)	107
Ir(4)−Ir(1)−Te(1)	145.41(6)	Ir−C_{term}−O_{term} (average)	176
Ir(6)−Ir(2)−Te(1)	146.93(6)	Ir−C(13)−O(13)	138
Ir(2)−Ir(3)−Te(2)	147.84(7)	(average)	

[a] Estimated standard deviations are given in parentheses.

opposite Ir(1)−Ir(3) edge. Instead, the bending of the phenyl residue in **2** reduces the symmetry of the whole anion to C_1. The average Ir−Ir distances are 2.764 Å in **2** and 2.761 Å in **3**. Average Ir−Te bonds are 2.615 Å in **2** and 2.613 Å in **3**.

Table 1 shows that the deformations of the metal octahedron in **2** are mainly located in the square section [Ir(1), Ir(2), Ir(4) Ir(5)] coplanar with the Ir_2Te unit: the longest bond of the framework is Ir(4)−Ir(5) (2.840(1) Å), opposite to the bridged edge, whereas the shortest are Ir(1)−Ir(5) (2.707(1) Å) and Ir(2)−Ir(4) (2.708(1) Å), which are almost *trans* to the Ir−Te bonds (Te−Ir−Ir angles of 145−149°). The edge bridged by tellurolate (2.738(1) Å) and those bridged by μ-CO (average 2.742 Å) are comparably short. Therefore, the bond lengths in **2** can be ordered as follows: bonds *trans* to tellurium < bond bridged by tellurium < bonds bridged by CO < bond opposite to tellurium. The same trend holds for **3** also, even if it is somehow hidden by the poorer quality of data and by the much more complex geometrical relationship of any edge with two different μ-TePh units. In $[Ir_6(CO)_{13}(\mu\text{-TePh})_2]$, the order of lengths of the corresponding Ir−Ir bond are as follows: bonds *trans* to tellurium (average 2.735 Å) < bonds spanned by μ-TePh (average 2.747 Å) < the unique edge bridged by CO (2.782(1) Å) < bonds opposite to the tellurium bridges (2.822 Å).

The new cluster $[Ir_6(CO)_{14}(\mu\text{-TePh})]^-$ fills the gap in the series $[Ir_6(CO)_{12}(\mu\text{-CO})_2(\mu\text{-X})]^-$, where X ($PPh_2$,[15] TePh, I, Br,[11] or Cl[12]) is a three-electron donor linked to the metals through atoms of groups 15−17: all of these complexes adopt the same octahedral structure with the same architecture of the carbonyl ligands, formally derived by the structure of D_3 symmetry of the unsubstituted $[Ir_6(CO)_{12}(\mu\text{-CO})_3]^{2-}$.[16] The Ir−Ir distances of the other $[Ir_6(CO)_{14}(\mu\text{-X})]^-$ clusters (the only exception being $[Ir_6(CO)_{14}(\mu\text{-Br})]^-$) follow an identical trend,[11,12,15] suggesting a constant influence of the main-group bridging atom. The more striking feature is, to our opinion, the shortening of the Ir−Ir bonds *trans* to Ir−X interactions.

Experimental Section

All of the solvents were purified and dried by conventional methods and stored under nitrogen. All of the reactions were carried out under oxygen-free nitrogen atmospheres using Schlenk-tube techniques.[17] $[PPh_4]_2[Ir_6(CO)_{15}]$[18] and $Ir_6(CO)_{16}$[19] were prepared by literature methods. Infrared spectra were recorded on a Perkin-Elmer 16 PC FT-IR spectrophotometer, using calcium fluoride cells previously purged with N_2. Elemental analyses were carried out by the staff of Laboratorio di Analisi of the Dipartimento di Chimica Inorganica, Metallorganica e Analitica. The mass peaks are referenced to the most abundant isotopomers; the agreement between the observed and calculated isotopic distributions were always excellent.

The materials and apparatus for the electrochemistry have been described elsewhere.[20] All potential values are referenced to the saturated calomel electrode. Under the present experimental conditions, the one-electron oxidation of ferrocene occurs at +0.39 V.

Synthesis of $[PPh_4][Ir_6(CO)_{14}(TePh)]$ (2a). $[PPh_4]_2[Ir_6(CO)_{15}]$ (0.33 g, 0.15 mmol) was dissolved in THF (10 mL), and three portions of PhTeTePh (0.08 g, 0.20 mmol each) were

(15) Della Pergola, R.; Brivio, E.; Garlaschelli, L.; Masciocchi, N.; Manassero, M. *J. Cluster Sci.* **1994**, *5*, 363.
(16) Demartin, F.; Manassero, M.; Sansoni, M.; Garlaschelli, L.; Martinengo, S.; Canziani, F. *J. Chem. Soc., Chem. Commun.* **1980**, 903.
(17) Shriver, D. F.; Dredzon, M. A. *The Manipulation of Air-Sensitive Compounds*, 2nd ed.; Wiley: New York, 1986.
(18) Angoletta, M.; Malatesta, L.; Caglio, G. *J. Organomet. Chem.* **1975**, *94*, 99.
(19) Garlaschelli, L.; Martinengo, S.; Bellon, P. L.; Demartin, F.; Manassero, M.; Chiang, M. Y.; Wei, C.-Y.; Bau, R. *J. Am. Chem. Soc.* **1984**, *106*, 6664.
(20) Barbaro, P.; Bianchini, C.; Laschi, F.; Midollini, S.; Moneti, S.; Scapacci, G.: Zanello, P. *Inorg. Chem.* **1994**, *33*, 1622.

added every 8 h while refluxing and monitoring by IR. When the reaction was completed, the deep red mixture was filtered. Addition of 2-propanol and concentration in vacuum induced precipitation of the crude product. The solid was collected by filtration, washed with 2-propanol (2 × 5 mL), and dried. It was then dissolved in a minimum amount of CH_2Cl_2, and the solution was layered with cyclohexane. Yield: 0.23 g (75%) of crystals suitable for X ray analysis. Anal. Calcd for $C_{44}H_{25}Ir_6O_{14}PTe$: C, 25.3; H, 1.21. Found: C, 25.6; H, 1.4. IR: ν(CO) 2060 w, 2018 vs, 2009 s, 1957 w, 1812 m cm^{-1} (in THF). FAB MS (negative ions): m/z 1751 ($[Ir_6(CO)_{14}TePh]^-$), 1751 − 28x ($[Ir_6(CO)_{14-x}TePh]^-$, x = 1−11).

Synthesis of $[Ir_6(CO)_{13}(TePh)_2]$ (3) from $Ir_6(CO)_{16}$. $[Ir_6(CO)_{16}]$ (0.38 g, 0.24 mmol) and PhTeTePh (0.12 g, 0.29 mmol) were suspended in toluene (10 mL) and refluxed while monitoring by IR. After 2 h, the reaction was completed and the solvent was dried in vacuum. The dark residue was purified by chromatography on silica (eluent acetone:hexane = 1:9). The green band (R_f = 0.54) was collected, and the solution was dried. The solid was dissolved in CH_2Cl_2, and the solution was layered with heptane. Yield: 0.15 g, 32%. Anal. Calcd for $C_{25}H_{10}Ir_6O_{13}Te_2$: C, 15.6; H, 0.5. The elemental analyses of the crystals vary slightly with time: on freshly isolated samples we found C, 16.6; H, 0.9. On aged crystals, we found C, 15.6; H, 0.4. These data are consistent with the ideal stoichiometry $[Ir_6(CO)_{13}(TePh)_2]\cdot 0.5C_7H_{16}$, the heptane being slowly released from the lattice. Anal. Calcd for $C_{28.5}H_{18}Ir_6O_{13}Te_2$: C, 17.3; H, 0.9. IR: ν(CO) 2077 m, 2046 vs, 2034 s, 2016 m, 1984 w, 1835 m cm^{-1} (in toluene). FAB MS (negative ions): m/z 1898 ($[Ir_6(CO)_{12}(TePh)_2]^-$), 1898 − 28$x$ ($[Ir_6(CO)_{12-x}(TePh)_2]^-$, x = 1−12). The parent peak at m/z = 1926 was not observed.

Synthesis of $[Ir_6(CO)_{13}(SeCH_2Ph)_2]$. The cluster $[Ir_6(CO)_{13}(\mu\text{-}SeCH_2Ph)_2]$ was obtained similarly from $Ir_6(CO)_{16}$ and $PhCH_2SeSeCH_2Ph$ in 36% yield. IR: ν(CO) 2080 m, 2047 vs, 2034 s, 2018 m, 1986 w, 1838 m cm^{-1} (in toluene). ^{1}H NMR (THF-d_8): δ 7.4 (5 H, C_6H_5), 4.9 (2 H, CH_2); the last signal appears as a AB system, suggesting hindered rotation around the Se−CH_2Ph bond. Small satellite peaks are probably due to ^2J(H−Se) coupling (^{77}Se, spin $^1/_2$, natural abundance 7.6%).

Synthesis of $[Ir_6(CO)_{14}(SPh)]^-$ and $[Ir_6(CO)_{13}(SPh)_2]$ from $[Ir_6(CO)_{15}]^{2-}$. $[PPh_4]_2[Ir_6(CO)_{15}]$ (0.37 g, 0.16 mmol) and PhSSPh (0.18 g, 0.8 mmol) were dissolved in CH_2Cl_2 (10 mL); solid $[Fe(C_5H_5)_2][PF_6]$ (0.11g, 0.33 mmol) was added, and the deep green solution was stirred for 2 h. Addition of hexane (10 mL) induced precipitation of $[PPh_4]PF_6$, which was eliminated by filtration. The solvent was eliminated in vacuum, and the crude cluster product $[Ir_6(CO)_{13}(SPh)_2]$ was extracted with toluene (3 × 2 mL), leaving the monoanionic cluster $[Ir_6(CO)_{14}(SPh)]^-$ as a residue, which was dissolved in THF and layered with cyclohexane (yield 88 mg, 26%). The toluene fractions were collected together and layered with 2-propanol, yielding 16 mg (5%) of the impure product $[Ir_6(CO)_{13}(SPh)_2]$, the elemental analyses being not satisfactory. IR: ν(CO) 2084 m, 2051 vs, 2040 s, 2024 m, 1990 w, 1840 m cm^{-1} (in toluene). Characterization data of $[Ir_6(CO)_{14}(SPh)]^-$. IR: ν(CO) 2064 m, 2021 vs, 2012 s, 1963 w, 1804 m cm^{-1} (in THF). FAB MS (negative ions): m/z 1683 ($[Ir_6(CO)_{14}SPh]^-$), 1683 − 28x ($[Ir_6(CO)_{14-x}SPh]^-$, x = 1−10). Anal. Calcd for $C_{44}H_{25}Ir_6O_{14}PS$: C, 26.5; H, 1.3. Found: C, 26.2; H, 1.0.

X-ray Data Collection and Structure Determination. Crystal data and other experimental details are summarized in Table 3. The diffraction experiments were carried out on an Enraf-Nonius CAD-4 diffractometer at room temperature using Mo Kα radiation (λ = 0.710 73 Å) with a graphite monochromator in the incident beam. The calculations were performed on an AST Power Premium 486/33 computer using the personal structure determination package[21] and the physical constants tabulated therein. A periodic monitoring of three standard reflections revealed a crystal decay, on X-ray exposure, which was evaluated as about 2.1% for **2a** and 3.0% for **3** (on intensities) at the end of data collection. The diffracted intensities were corrected for Lorentz, polarization, decay, and absorption effects (empirical correction).[22] Scattering factors and anomalous dispersion corrections were taken from ref 23. The structure were solved by direct methods (MULTAN)[24] and difference Fourier syntheses and refined by full-matrix least-squares, minimizing the function $\sum w(F_o - k|F_c|)^2$. Anisotropic thermal factors were refined for all non-hydrogen atoms. In all cases, the hydrogen atoms were placed in their ideal positions (C−H = 0.97 Å, B = 1.15 times that of the carbon atom to which they are attached) and not refined. The final Fourier map showed maximum residuals of 1.5(2) e Å^{-3} at 1.02 Å from Ir(5) in **2a** and 2.2(4) e Å^{-3} at 1.05 Å from Ir(1) in **3**.

Table 3. Crystal Data and Data Collection Parameters

compd	**2a**	**3**
formula	$Ir_6TePO_{14}C_{44}H_{25}$	$Ir_6Te_2O_{13}C_{25}H_{10}$
fw	2089.46	1926.75
color	black	black
cryst syst	triclinic	monoclinic
space group	$P\bar{1}$ (No. 2)	$C2/c$ (No. 15)
a, Å	9.921(2)	16.199(4)
b, Å	14.935(3)	10.043(3)
c, Å	16.818(3)	43.576(13)
α, deg	94.43(2)	
β, deg	98.79(2)	91.43(2)
γ, deg	101.29(2)	
V, Å^3	2400.2(9)	7087(5)
Z	2	8
F(000)	1860	6640
D_{calcd}, g cm^{-3}	2.891	3.611
cryst dimens	0.28 × 0.45 × 0.50	0.08 × 0.28 × 0.40
μ(Mo Kα), cm^{-1}	172.0	240.4
min. transm. fact.	0.46	0.15
scan mode	ω	ω
ω-scan width, deg	1.00 + 0.35 tan θ	1.20 + 0.35 tan θ
θ-range, deg	3−25	3−25
octants of reciprocal space explored	+h, ±k, ±l	+h, +k, ±l
no. of measd reflns	8388	6213
no. of unique obsd reflns with $I > 3\sigma(I)$	6425	4051
final R and R_w[a]	0.034, 0.048	0.055, 0.078
no. of variables	596	415
GOF[b]	1.34	1.91

[a] $R = [\sum(F_o - k|F_c|)/\sum F_o]$; $R_w = [\sum w(F_o - k|F_c|)^2/\sum wF_o^2]^{1/2}$. [b] GOF = $[\sum w(F_o - k|F_c|)^2/(N_{obsns} - N_{var})]^{1/2}$, $w = 1/(\sigma(F_o))^2$, $\sigma(F_o) = [\sigma^2(I) + (0.06I)^2]^{1/2}/2F_oLp$.

Acknowledgment. P.Z. acknowledges the financial support of CNR and Human Capital and Mobility Programme (EC Contract No. CHRX-CT93-0277) and the technical assistance of Mrs. G. Montomoli.

Supporting Information Available: Tables of atomic coordinates, anisotropic thermal parameters (U) for the non-hydrogen atoms, and complete bond distances and angles for compound **2a** and **3** and a cyclic voltammogram recorded in CH_2Cl_2 solution containing $[Ir_6(CO)_{15}]^{2-}$ and PhSSPh (18 pages). Ordering information is given on any current masthead page.

OM970621+

(21) Frenz, B. A. *Comput. Phys.* **1988**, *2*, 42; *Ibid., Crystallographic Computing* 5; Oxford University Press: Oxford, U.K., 1991; Chapter 11, p 126.

(22) North, A. C. T.; Phillips, D. C.; Mathews, F. S. *Acta Crystallogr., Sect. A* **1968**, *24*, 351.

(23) *International Tables for X-ray Crystallography*; Kynoch Press: Birmingam, U.K., 1974.

(24) Main, P.; Fiske, S. J.; Hill, E.; Lessinger, L.; Germain, G.; Declercq, J. P.; Wolfson, M. M. *MULTAN 80, a system of computer programs for the automatic solution of crystal structures from X-ray diffraction data*; Universities of York and Louvain: U.K. and Belgium, 1980.